Seasonal variability of neutral escape from Mars as derived from MAVEN pickup ion observations

A. Rahmati[1], D. E. Larson[1], T. E. Cravens[2], R. J. Lillis[1], J. S. Halekas[3], J. P. McFadden[1], D. L. Mitchell[1], E. M. B. Thiemann[4], J. E. P. Connerney[5], P. A. Dunn[1], C. O. Lee[1], F. G. Eparvier[4], G. A. DiBraccio[5], J. R. Espley[5], J. G. Luhmann[1], C. Mazelle[6], and B. M. Jakosky[4]

[1]Space Sciences Laboratory, University of California, Berkeley, California, USA.

[2]Department of Physics and Astronomy, University of Kansas, Lawrence, Kansas, USA.

[3]Department of Physics and Astronomy, University of Iowa, Iowa City, Iowa, USA.

[4]Laboratory for Atmospheric and Space Physics, University of Colorado, Boulder, Colorado, USA.

[5]NASA Goddard Space Flight Center, Greenbelt, Maryland, USA.

[6]IRAP/CNRS, Toulouse, France.

Corresponding author: Ali Rahmati (rahmati@ssl.berkeley.edu)

Key Points:

- Pickup ion measurements of SEP, SWIA, and STATIC on MAVEN constrain neutral escape rates of hydrogen and oxygen.
- Thermal hydrogen escape varies dramatically with Mars season from 3×10^{25} s^{-1} near aphelion to 4×10^{26} s^{-1} near perihelion.
- Hot oxygen escape remains constant with time to within a factor of two, with a mean value of 9×10^{25} s^{-1}.

This article has been accepted for publication and undergone full peer review but has not been through the copyediting, typesetting, pagination and proofreading process which may lead to differences between this version and the Version of Record. Please cite this article as doi: 10.1029/2018JE005560

Abstract

The Mars Atmosphere and Volatile EvolutioN (MAVEN) spacecraft arrived at Mars with the goal of determining the rates and mechanisms of atmospheric escape. Thermal hydrogen and hot oxygen escape are the two most important escape processes currently at work. Direct measurement of the escaping neutral hydrogen and oxygen atoms is impossible with current technology due to the low density and energy of escaping neutrals. However, when ionized and picked up by the solar wind, these escaping atoms can be detected by three particle detectors onboard MAVEN. By back-tracing the trajectories of measured pickup ions, constraints can be placed on the density of neutrals at altitudes not accessible by other measurement methods. In this work, pickup H^+ and O^+ data from the Solar Energetic Particle (SEP), Solar Wind Ion Analyzer (SWIA), and SupraThermal and Thermal Ion Composition (STATIC) instruments are used to assess the variability of neutral H and O exospheres at Mars. From an analysis of 2.5 Earth years of MAVEN data, we show that a strong H escape seasonal dependence is observed by SWIA and STATIC with inferred H escape rates as low as 3×10^{25} s^{-1} near aphelion and as high as 4×10^{26} s^{-1} near perihelion. Hot O escape rates derived from SEP, SWIA, and STATIC data imply a much less variable hot O exosphere with escape rates fluctuating by a factor of 2 around a mean value of 9×10^{25} s^{-1}. Both escape rates are in general agreement with the most recent theoretical, modeled, and observationally inferred rates.

1. Introduction

Mars has lost most of its atmosphere, as evidenced by studies that suggest the planet was warm and wet in the past, with an atmosphere that was able to support water in liquid form on the surface [e.g., Jakosky et al., 1994; Chassefière and Leblanc, 2004; Jakosky et al., 2017; Kurokawa et al., 2018]. The main objectives of the MAVEN (Mars Atmosphere and Volatile EvolutioN) mission to Mars are to determine the current state of the Mars upper atmosphere, understand the mechanisms leading to the loss of Mars's atmosphere to space, and study the response of the atmosphere to the processes controlling it [Jakosky et al., 2015a,b; Bougher et al., 2014, 2015; Lillis et al., 2015]. Currently, the major pathways for atmospheric loss on Mars are thermal escape of neutral hydrogen atoms (Jeans escape) [e.g., Hunten and McElroy, 1970] and photochemical escape of neutral oxygen atoms (hot O escape) [e.g., Nagy and Cravens, 1998]. Over millions of years, these neutral escape channels

along with other forms of atmospheric escape, including ion outflow, sputtering, and pickup ion escape, have led to the disappearance of liquid water on Mars [e.g., Luhmann et al., 1992; Curry et al., 2013; Cravens et al., 2017; Dong et al., 2017; Dubinin et al., 2017; Ramstad et al., 2017; Johnson et al., 2018]. In the past, the neutral escape rates have been inferred from remote sensing via ultraviolet (UV) scattered and stimulated emissions from the upper atmosphere [e.g., Feldman et al., 2011; Chaffin et al., 2014]. These methods heavily rely on the deconvolution of line-of-sight, sometimes optically thick, measurements using exospheric models. While data-validated models of the hot oxygen and thermal hydrogen exosphere can be used together with UV spectrometer derived altitude profiles to infer the escaping components, in-situ measurements provide an alternative method. With the arrival of MAVEN at Mars, we have been able to use an alternative approach, described below, that takes advantage of its especially comprehensive combination of in-situ measurements. The present report describes new insights based on the application of this method following the acquisition of over a Mars-year of orbital sampling.

Directly measuring the rate of escaping neutrals from Mars is not possible with current technology. This is because, on the one hand, the escaping neutrals in the Mars exosphere have very low energies (below a few eV) and very low densities (below 100 cm^{-3} above 3,000 km altitude). On the other hand, the escaping neutrals are heavily dominated in density, up to several Mars radii (1 R_M ~ 3400 km), by neutral atoms that are gravitationally bound to the planet and thus not escaping. Rahmati et al. [2014] showed that the escaping part of the hot oxygen exosphere at Mars becomes dominant at altitudes above ~10 R_M. Chamberlain models of the thermal hydrogen exosphere assuming a Maxwellian distribution at the exobase also show that bound hydrogen is dominant up to tens of R_M [Chamberlain and Hunten, 1987]. Direct measurement of exospheric ionized atoms is, however, possible with the current charged particle detectors. Hydrogen and oxygen atoms in the Mars exosphere can be ionized by photoionization, charge exchange with solar wind protons, and electron impact ionization. These ions respond to the solar wind fields and are picked up by the solar wind motional electric field, accelerating them to energies high enough to be measurable by charged particle detectors. These pickup ions can be used to extract information about their source neutrals, such as neutral densities and escape rates.

Barabash et al. [1991] and Dubinin et al. [2006] used hydrogen pickup ion measurements from the Phobos 2 and the Mars Express spacecraft, respectively, to put constraints on the hydrogen exospheric densities at Mars. Cravens et al. [2002] analyzed

oxygen pickup ions measured by the solid state telescope on the Phobos 2 spacecraft and showed that pickup O^+ fluxes can be used to constrain the hot oxygen exosphere of Mars. Rahmati et al. [2014] similarly showed that the SEP (Solar Energetic Particle) instrument on MAVEN can also detect pickup O^+ ions when the solar wind speed is high enough for pickup ions to reach energies above ~60 keV. They also demonstrated that the SEP-measured oxygen pickup ions are created in the far reaches of the exosphere of Mars, where the escaping part of the neutral O exosphere is dominant, thus allowing neutral oxygen escape rates to be constrained. Rahmati et al. [2015] confirmed with MAVEN data that SEP is indeed able to measure pickup O^+ and successfully reproduced SEP-measured pickup ion spectra with a pickup ion model. Rahmati [2016] showed that SWIA (Solar Wind Ion Analyzer) and STATIC (SupraThermal and Thermal Ion Composition) on MAVEN can also detect both pickup H^+ and O^+ and provided several model-data comparisons for different upstream conditions. Rahmati et al. [2017] used SEP, SWIA, and STATIC-measured pickup ions to study two MAVEN orbits, one near Mars perihelion and one near Mars aphelion, and found that the hot O exosphere changed by less than a factor of 2 between the two orbits, whereas the thermal H exosphere dropped by an order of magnitude from perihelion to aphelion. This latter work suggested that there are quite different seasonal dependences of the H and O escape rates, a topic we pursue here with a more comprehensive analysis using a larger data base.

In this work, all pickup ion data measured by SEP, SWIA, and STATIC taken during just over one Mars year (the first 2.5 Earth years of MAVEN's science phase) are studied for the time periods when MAVEN was in the solar wind and upstream parameters were available to model pickup ions. The data are compared with simulation results from the pickup ion model described below to derive the variability of neutral escape from Mars. Section 2 describes the pickup ion model used in this study and explains how neutral escape rates are derived from pickup ion data-model comparisons. Section 3 details the MAVEN data used in this study, Section 4 examines the variability found in neutral escape rates, and Section 5 discusses each escape mechanism and provides comparisons with previous work, including results derived from UV remote sensing techniques.

2. Pickup Ion Model

Pickup ions that are created in the exosphere of Mars via ionization of neutral atoms are energized by the solar wind motional electric field and follow cycloidal trajectories. The production and transport of these pickup ions can be simulated given knowledge of the ionization rates and solar wind fields. Fortunately, MAVEN carries instrumentation that measures all of the parameters required to carry out this analysis. Rahmati et al. [2015, 2017] and Rahmati [2016] extensively described the pickup ion model used in this study and showed that the model is successful in reproducing the angular and energy dependence of pickup ions measured by SEP, SWIA, and STATIC. A brief description of the model is given below.

The pickup ion model calculates ionization rates of neutrals and analytically solves for the trajectories of pickup ions, then convolves pickup ion fluxes with each instrument response in order to mimic what each instrument measures. The MAVEN particle detectors each have their own characteristic energy and angular response, geometric factor, look direction, and field of view, as described by Larson et al. [2015], Halekas et al. [2015], and McFadden et al. [2015]. Rahmati et al. [2017] provide comparisons of the measured and modeled pickup ion energy spectra for SEP, SWIA, and STATIC in a few look directions and over the energy coverage of each instrument. The neutral source positions of pickup ions are calculated in the model by back-tracing the measured pickup ion trajectories. Although pickup ion spectra are typically calculated by integrating pickup ion fluxes along their trajectories, the pickup ion flux measured in a single energy and angular bin of each instrument is directly proportional to the neutral density in the immediate vicinity of the location where the measured pickup ion was created. By comparing the measured and modeled pickup ion fluxes, the source density of pickup ions, i.e., the density of neutral atoms in the exosphere of Mars where neutral escape is happening, can be derived, thus constraining neutral escape rates.

To reliably model the whole pickup ion dataset measured by MAVEN, the following criteria are considered: The time periods when MAVEN was in the solar wind are selected to be far enough from the nominal location of the bow shock to ensure that MAVEN is located in the undisturbed solar wind for most of the analyzed time periods. This, however, does not guarantee the exclusion of disturbed conditions caused by the foreshock, which can extend many R_M upstream of the bow shock. The pickup ion model averages the data input parameters discussed in the next section over a 64 s time period. For each 64 s time bin, 3000

particles are simulated, resulting in a reasonably smooth modeled pickup spectrum. For adequate statistics, the model ensures that there are at least 3 test particles per simulated gyro-period in each instrument energy and angular bin. The total number of particles was selected based on a compromise between model accuracy and simulation run time. Pickup H^+ gyro-radii typically range between 300 and 3000 km depending on upstream conditions; therefore several pickup H^+ gyro-periods need to be simulated in the model to ensure that the whole neutral hydrogen exosphere is captured as a source for pickup ions. For the same solar wind parameters, pickup O^+ gyro-radius is 16 times that of pickup H^+; thus one gyro-period for pickup O^+ is enough for capturing the whole oxygen exosphere. For SEP, SWIA, and STATIC, the lowest level of energy fluxes, i.e., background counts, are removed from model-data comparisons in order to eliminate any background noise artifacts.

Hydrogen and oxygen neutral escape rates are inferred from MAVEN pickup ion measurements by comparing the detected flux of pickup ions in each instrument with the flux that the pickup ion model predicts based on an assumed neutral exosphere. The neutral density profiles fed into the model and later adjusted based on measured pickup ion data are taken from Feldman et al. [2011] for H and Rahmati et al. [2014] for O, as shown in Figure 2a of Rahmati et al. [2017]. The neutral escape rates associated with these density profiles are 6×10^{25} s^{-1} for H and 7×10^{25} s^{-1} for O. By assuming a constant exobase temperature for H, and also assuming that the energy dependence of the distribution function of O at the exobase stays constant with time, the neutral escape rates will only scale with the exospheric neutral densities. Therefore, the scale factor used to adjust the density profiles fed into the pickup ion model in order to fit the measured pickup ion fluxes is the same factor that adjusts the escape rates. The scale factors determined from pickup ion data-model comparisons and their variability with time as determined by MAVEN measurements are provided in Section 4. The assumption of a constant exobase temperature for H is not necessarily a valid one and the amount to which the exobase temperature variations can affect the interpretations of this work is briefly discussed in Section 5.1.

3. MAVEN Data

MAVEN carries nine science instruments that measure the solar wind, solar irradiance, and energetic particle input to the Mars atmosphere, as well as the reaction of the

atmosphere to those inputs. In this work, data from six MAVEN instruments are used to derive neutral escape rates:

3.1. MAG [Connerney et al., 2015]

The magnetometer on MAVEN measures the 3 components of the vector magnetic field at a maximum sampling rate of 32 Hz. Both the magnitude and the direction of the measured magnetic field in the solar wind are used in the pickup ion model to calculate pickup ion trajectories. The daily averaged magnitude of the IMF is shown in panel 1 of Figure 1. It is seen that there are five time periods during which part of the MAVEN orbit was consistently outside the bow shock, enabling measurement of upstream solar wind parameters.

3.2. SWIA [Halekas et al., 2015, 2017]

The SWIA instrument is an electrostatic analyzer that measures 3D distributions of ions from 25 eV to 25 keV. When MAVEN is in the solar wind, SWIA is able to accurately measure the upstream ion moments. The three components of the solar wind velocity are used in the pickup ion model to calculate pickup ion trajectories. The 2nd panel of Figure 1 shows the daily averaged solar wind speeds measured by SWIA. The solar wind densities, shown in panel 3 of Figure 1, are used in calculating the charge exchange rate of exospheric neutrals with solar wind protons. The charge exchange frequencies for H and O are calculated using measured solar wind fluxes and depicted by the red lines in panels 4 and 5 of Figure 1, respectively. As seen in the figure, charge exchange by solar wind protons is the dominant ionization process for hydrogen atoms. SWIA also measures H^+ and O^+ pickup ions and the output of our pickup ion model is ultimately compared with SWIA pickup ion measurements in order to derive neutral escape rates.

3.3. SWEA [Mitchell et al., 2016]

The SWEA (Solar Wind Electron Analyzer) instrument measures the suprathermal electron spectrum between 3 eV and 4.6 keV. The solar wind electron energy spectra measured by SWEA are corrected for spacecraft potential and used to calculate electron impact ionization rates of exospheric neutrals. The electron impact ionization frequencies for H and O are shown as green lines in panels 4 and 5 of Figure 1, respectively. Note that during early 2016, the SWEA instrument intermittently stopped sending data packets, causing the

gap seen in electron impact data in the aforementioned panels. As seen, solar wind electron impact is a minor source of ionization in the solar wind for both H and O.

3.4. EUVM [Eparvier et al., 2015]

The EUVM (Extreme UltraViolet Monitor) instrument measures the solar extreme ultraviolet irradiance in 3 wavelength channels. The FISM (Flare Irradiance Spectral Model) takes the EUVM measurements and constructs the full EUV spectrum from 0 to 190 nm in 1 nm bins [Thiemann et al., 2017]. The FISM spectra are used in calculating photoionization rates of exospheric neutrals. The blue lines in panels 4 and 5 of Figure 1 show photoionization frequencies for H and O, respectively. The modulation in photoionization frequencies is due to a combination of solar rotation, solar activity, and the Sun-Mars distance. As seen, photoionization is generally the dominant process for ionizing oxygen atoms; however, at times of high solar wind flux, charge exchange can dominate photoionization.

3.5. SEP [Larson et al., 2015]

The SEP instrument is designed to measure solar energetic particles, an important source of energy input into the Mars atmosphere. SEP's lower energy threshold for detection of H^+ and O^+ is ~ 20 keV and 60 keV, respectively. There are two SEP sensors on MAVEN, namely SEP1 and SEP2 that have look directions perpendicular to each other. In its forward look directions, SEP is able to measure oxygen pickup ions that are created several R_M upstream of Mars and have gained energies above 60 keV [Rahmati et al., 2015]. This energy threshold requires the solar wind speed to be greater than 500 km/s for SEP to be able to reliably detect pickup O^+. Since upstream pickup H^+ energies are generally below 10 keV, SEP cannot measure them and can therefore only be used to constrain hot O escape rates. Since solar energetic particles can contaminate measurements of pickup O^+, periods of solar energetic events are not included in our analysis.

3.6. STATIC [McFadden et al., 2015]

STATIC is an electrostatic analyzer that measures 3D ion distributions and includes a time of flight system that separates ions based on their mass to charge ratio. Due to data downlink limitations, STATIC data are down-sampled in energy, look direction, mass, and time. The STATIC data products that include mass resolved measurements in 8 mass channels and 64 look directions are named D0 and D1, the latter of which includes higher

time resolution data, but only available during burst data downlinks. STATIC detects pickup H^+ and O^+ with energies up to 30 keV in the aforementioned data products' 1st and 5th mass channels, respectively. Similar to SWIA, STATIC's pickup ion measurements can be used to constrain neutral H and O escape rates.

4. Variability of Neutral Escape Rates

Once our pickup ion model simulates the pickup ion fluxes that SEP, SWIA, and STATIC measure, the model then takes the ratio between the measured and model predicted fluxes for each look direction and energy bin to calculate how much the input neutral density profiles need to be adjusted to match the pickup ion data. Figure 2 shows the daily averaged pickup ion flux data to model ratios calculated for H and O averaged over all of the look directions and energy bins of the three instruments. As described in Section 2, the pickup ion flux data to model ratios are the same scale factors that need to be applied to the escape rates associated with the assumed input density profiles. For instance, a data to model ratio of 10 for pickup H^+ means that the assumed neutral H escape rate of 6×10^{25} s^{-1} in the model is too low by a factor of 10, and that the actual derived H escape rate from data-model comparisons would be 6×10^{26} s^{-1}.

Panels 1 and 2 in Figure 2 show the derived scale factors for H and O from STATIC and SWIA pickup ion measurements. It is seen that the time variations in STATIC and SWIA generally agree with each other, but the absolute values differ, at times, by as much as a factor of 2. The disagreement is possibly partly associated with the lack of reliable calibration between the two instruments at pickup ion energies. The instruments are typically calibrated in the Mars magnetosheath at energies at and below the solar wind proton energy (~ 1 keV), whereas pickup H^+ can gain energies as high as 4 times the solar wind proton energy. Pickup O^+ energies, on the other hand, can go up to as high as 64 times the solar wind proton energy, at times exceeding the upper energy detection limit of SWIA and STATIC. Moreover, the multichannel plates used in SWIA and STATIC utilize different technologies and have different energy dependent gains. In addition to the energy response of the instruments, the angular response of each instrument to the pickup ion ring-beam distribution can also play a role in causing disagreements between the measurements. The geometric factors used to convert SWIA and STATIC counts to physical units assume that the angular width of each look direction is fully covered with the incoming flux of particles, whereas the ring

distribution of pickup ions only partially covers each look direction. This can lead to systematic differences in the measured differential fluxes between SWIA and STATIC depending on how the pickup ion ring orients with respect to each look direction as well as on the angular resolution of each instrument. No correction factor for the energy and angular response of SWIA and STATIC has been utilized in this work in order to remedy the disagreement between the two instruments. Nevertheless, both instruments imply an order of magnitude change in the H escape rates (panel 1), whereas the O escape rate remains constant to within a factor of 2 (panel 2) over the 2.5 Earth years of observations.

The 3rd panel in Figure 2 shows neutral O escape scale factors from SEP1 and SEP2 forward look directions as derived from pickup O^+ flux data to model ratios. Each point in the panel corresponds to the averaged scale factor over 1 day. The reason there are only a few points during late 2015 and early 2016 is because the solar wind speed stayed below 500 km/s for most of that time period, as seen in panel 2 of Figure 1, precluding reliable detection of pickup O^+ (see Section 3.5). The higher scatter in SEP derived scale factors compared to SWIA and STATIC is due to the lower number of SEP pickup ion data points available during each single day. This is because, in addition to requiring higher solar wind speeds, each SEP's field of view only covers about 3% of the sky, missing most of the pickup O^+ ring-beam distribution. SWIA and STATIC, on the other hand, detect pickup ions over a much wider field of view, up to 70% of the sky in 64 look directions, although this spatial coverage is reduced for energies above 5 keV. Nonetheless, similar to SWIA and STATIC, the trend seen in the SEP derived O escape scale factors implies that the hot O escape rates do not vary as dramatically as the derived thermal H escape rates.

The last two panels of Figure 2 show the heliocentric distance of Mars and its solar longitude, respectively. As seen, the largest H escape scale factors happen close to perihelion and drop by an order of magnitude near aphelion. This factor of 10 change in H escape is consistent with what Rahmati et al. [2017] found using the same method by analyzing two orbits, one near perihelion, and one near aphelion. In order to come up with actual escape rates in physical units, the scale factors have to be multiplied with the escape rates associated with the neutral density profiles used as input in the pickup ion model. Figure 3 accomplishes this by showing weekly averaged neutral H and O escape rates versus solar longitude. For H, SWIA and STATIC data are averaged, and for O, SWIA, STATIC, SEP1, and SEP2 are averaged to come up with a single weekly averaged escape rate for each species. Neglecting the few outliers, the O escape rate stays constant to within a factor of 2, fluctuating around an

average value of 9×10^{25} s^{-1}. Between $L_s = 0°$ and 180°, oxygen seems to dominate hydrogen in neutral escape at Mars, a trend which is reversed after Mars crosses $L_s = 180°$. H escape varies by an order of magnitude with season dropping to as low as 3×10^{25} s^{-1} near aphelion and rising to as high as 4×10^{26} s^{-1} near perihelion. The maximum H escape appears to happen at or just after southern summer solstice.

Some of the fluctuations seen in the derived neutral escape rates are most likely due to the rapid spatial and temporal variability of the upstream conditions, and not representative of the actual changes in the neutral escape rates. Pickup H^+ gyro-periods typically range between 6 and 60 seconds depending on upstream conditions and pickup O+ gyro-periods are 16 times that. Any variability in upstream conditions on timescales less than the pickup gyro-periods will results in modeled fluxes that will not match the data. Any deviation in the measured magnetic field and solar wind velocity translates to an error in the calculated pickup trajectories in the model, placing the test particles in wrong instrument look directions and energy bins. For instance, the significant jump in the O escape rate at $L_s = 40°$ is likely due to the uncertainties in the measured upstream parameters, since the uncertainties are highest near the edges of the time periods with upstream solar wind access. This is because the least amount of time is spent by MAVEN in the solar wind just before and after completely losing solar wind coverage and also MAVEN is more likely to be in the foreshock when in close proximity of the bow shock.

Since pickup O^+ gyro-radii are several R_M, simulating a single gyro-period for pickup O^+ is enough to capture the entire hot O exosphere. This enables us to back-trace the measured oxygen pickup ions in a single look direction and energy bin to a single birth point in the exosphere. We can therefore reconstruct hot O density profiles based on pickup O^+ model-data comparisons. Figure 4 shows three hot O density profiles derived from SEP, SWIA, and STATIC pickup O^+ measurements averaged over all of the available data, along with the hot O density profile of Rahmati et al. [2014]. Given the same methodology used in this work and that of Rahmati et al. [2017], the standard deviations in the derived densities are similar to what Rahmati et al. [2017] found, purely calculated from the variations of the retrieved densities and spanning over almost an order of magnitude in density between one standard deviation below and above the mean. The standard errors of the mean densities, however, are less than 10% due to the much larger dataset used to derive the density profiles compared to Rahmati et al. [2017]. It is seen that due to its large geometric factor, SEP can be used to constrain densities at altitudes as high as 200,000 km (~ 60 R_M) where the hot O

density is less than 1 cm^{-3}. The reason SEP cannot measure pickup O^+ that is born below ~15,000 km in altitude is due to SEP's 60 keV lower energy threshold requirement for detection of O^+, as newly born oxygen pickup ions need such distance to gain as least 60 keV by the solar wind motional electric field. SWIA and STATIC, however, can constrain hot O densities from altitudes as low as 4000 km to as high as 70,000 km for SWIA and 50,000 km for STATIC. The reason STATIC can constrain hot O densities up to a lower maximum altitude compared to SWIA is due to its smaller geometric factor. The factor of 3 disagreement in the density profiles derived from the three instruments can again be associated with calibration issues, as the instruments have not been calibrated against each other for the purpose of measuring pickup ions.

Rahmati et al. [2017] provided reconstructed density profiles for two MAVEN orbits for both O and H, but mentioned that the derived H density profiles could have been overestimated by as much as 30% due to factor of 16 smaller gyro-radius of pickup H^+ compared to pickup O^+. This is because for certain upstream parameter values, more than one pickup H^+ gyro-period needs to be simulated in the model to calculate total pickup fluxes. This means that unlike pickup O^+, not all of the measured pickup H^+ can be traced back to a single neutral source position. This creates some ambiguity in reconstructing H density profiles for time periods longer than an orbit, where gyro-radii can change by up to an order of magnitude due to variations in the solar wind velocity and magnetic field. Consequently, care must be taken in reconstructing H density profiles for the whole mission using this pickup ion technique in an automated fashion, and each orbit needs to be evaluated on a case by case basis.

5. Discussion and Conclusions

The continuous and comprehensive measurements made by the MAVEN suite of particle and field instruments have paved the way in understanding the escape mechanisms currently at work in the atmosphere of Mars. The variability in the escape rates of neutral H and O derived in this work by using our pickup ion technique is generally consistent with the most recent models and inferred rates from data of neutral escape from Mars, as discussed below.

5.1. Thermal H Escape Variability

The hydrogen exosphere of Mars has been under study for almost half a century, starting with the Mariner 6, 7, and 9 missions [Anderson, 1974]. The larger than expected range of variability in the escape rate of neutral hydrogen from Mars has, however, only come to light in the past few years. Clarke et al. [2014] used Hubble Space Telescope (HST) observations of the scattered solar Ly α emission and found a 40% steady decrease in hydrogen corona over the span of 4 weeks beginning in mid-October 2007. Similar longer term HST observations along with a radiative transport analysis by Bhattacharyya et al. [2015, 2017] implied an order of magnitude change in H escape rates with Mars season. Chaffin et al. [2014] used Mars Express Ly α observations and also found an order of magnitude drop in the H escape rate from July 2007 to January 2008. The Imaging Ultraviolet Spectrograph (IUVS) instrument on MAVEN has also been used to study the H corona [Chaffin et al., 2015]. The echelle spectrograph channel of IUVS was used by Clarke et al. [2017] and Mayyasi et al. [2017] to study the variations in H and D emissions, which found that both emissions vary by an order of magnitude over one Mars year.

In addition to the spectroscopic techniques discussed above, Halekas [2017] used the flux of double charge exchanged precipitating protons measured by SWIA and inferred the same order of magnitude variation in H escape rates. The proton cyclotron wave analysis of Bertucci et al. [2013] and Romanelli et al. [2016], as well as the variations found in the pickup H^+ fluxes measured by MEX [Yamauchi, 2015] also suggest a dynamic H exosphere that varies dramatically with season. Recent modeling efforts also attempt to explain the factor of 10 change in H escape flux by using a 3D General Circulation Model [Chaufray et al., 2015] and by introducing high-altitude water in a 1D time-dependent photochemical model [Chaffin et al., 2017]. Heavens et al. [2018] recently showed that such high-altitude water vapor, driven by dust activity in the lower and middle atmosphere, does indeed correlate with large increases in H escape rate.

The results of this work are in general agreement with the findings of the aforementioned studies, pointing to a strong seasonal dependence of H escape from Mars. The neutral H density profile used as an input to the pickup ion model in this work was assumed to have a constant exobase temperature of 200 K, consistent with the Feldman et al. [2011] derived H profile. The exobase density was therefore the only free parameter used in fitting the data. As Halekas [2017] shows, increasing the exobase temperature from 200 K to 800 K can enhance the escape rates by more than an order of magnitude. Bhattacharyya et al.

[2015, 2017] introduced a second 800 K component to their thermal H model for a better fit to the HST data and found escape rates that were as much as two times higher than their one-component model. Our goal in this work was to put constraints on the amount of H escape variability using our pickup ion technique. We found that H escape varies with Mars season by an order of magnitude ranging between 3×10^{25} s^{-1} and 4×10^{26} s^{-1}. In future work attempts will be made to explore the effect on H escape rates of employing a multi-component exosphere with variable exobase temperatures.

5.2. Hot O Escape Variability

Over the past few decades, several models have investigated the variability of hot O escape from Mars as a function of solar EUV and solar wind input [e.g., Kim et al., 1998; Kaneda et al., 2009, Valeille et al., 2009; Cravens et al., 2016]. The most recent observations of the Mars hot O corona by MAVEN IUVS [Deighan et al., 2015] and the subsequent successful comparison with the 3D hot O corona model of Lee et al. [2015] show promise in constraining the variability of the hot O exosphere using MAVEN coronal ultraviolet measurements. Lillis et al. [2016] used MAVEN in situ measurements to calculate local hot O production rates from the O_2^+ dissociative recombination along with the probability that the produced hot O atoms will escape the planet. They found escape rates that range from 1.2 to 5.5×10^{25} s^{-1} with an EUV irradiance dependence that is somewhat stronger than the linear dependence predicted from the simple analytical scaling of Cravens et al. [2016]. Our derived average neutral oxygen escape rate is 9×10^{25} s^{-1}, with a factor of 2 fluctuation in time that is most likely caused by uncertainties in the upstream measurements, rapid fluctuations of upstream fields on timescales less than a pickup gyro-period, and foreshock effects disturbing the upstream solar wind. The hot O exosphere itself is most likely steadier in time and varies on timescales on the order of seasonal changes in the EUV irradiance.

The EUV irradiance input to the Mars atmosphere is thought to be the main driver of hot O escape variability [Cravens et al., 2016 and references therein]. The EUV irradiance at Mars, however, varied by less than a factor of 2 due to solar activity and Mars' heliocentric distance variations during the analyzed period [Lillis et al., 2016]. The results of this work also suggest that hot O escape varies by less than a factor of 2 with Mars season, supporting the previous model and analytical predictions that there should be a linear relationship between the EUV irradiance and hot O escape. Our pickup ion analysis is the only technique thus far that can gain access to hot O neutral densities at altitudes where the escaping part of

the exosphere is dominant. Although the hot O neutral densities and escape rates derived from SEP, SWIA, and STATIC differ from each other by as much as a factor of 3 due to possible calibration issues, each instrument alone implies a variability in hot O escape that is in line with the theoretical work of Cravens et al. [2016].

MAVEN arrived at Mars as the current weak solar cycle was just starting its declining phase and approaching minimum solar activity, thus it should be noted that the inferred escape rates in this work do not cover the whole range of possible EUV variations. It remains to be determined whether a stronger variation in EUV irradiance would result in hot O variations that can be revealed with statistical significance using our pickup ion technique. We also have not considered the possible enhanced exosphere responses to stormy space weather conditions when ionization rates may increase and sputtering may contribute a more significant additional component of the neutral exosphere.

5.3. Summary and Future Work

In Summary, we used pickup ion data from the SEP, SWIA, and STATIC instruments on MAVEN to constrain escape rates of neutral hydrogen and oxygen. We found that thermal hydrogen escape varies dramatically with Mars season from 3×10^{25} s^{-1} near aphelion to 4×10^{26} s^{-1} near perihelion. Hot oxygen escape, however, remains constant with time to within a factor of two, with a mean escape rate of 9×10^{25} s^{-1}.

In future work, we will attempt to reconcile the factor of 3 disagreement between SEP, SWIA, and STATIC derived neutral escape rates by inspecting the calibration between the three instruments for detection of pickup ions. We also seek to use a more robust algorithm to minimize the inclusion of disturbed upstream parameters that result in errors in our pickup ion simulation. As more data becomes available in the future, we will investigate whether the same seasonal trend in the variation of H and O escape will be seen in multiple Mars years. With more statistics in hand, we will explore the EUV dependence of hot O escape and will also study the impact of a varying exobase temperature and distribution function on our derived H and O escape rates. As more spatial coverage in pickup ion trajectories is obtained, we will be able to reconstruct the 3D structure of the neutral exosphere and examine the degree to which the exosphere of Mars is isotropic. Finally, we will assess the impact that extreme space weather conditions will have on the neutral exosphere of Mars.

Acknowledgments and Data

The MAVEN project is supported by NASA through the Mars Exploration Program. MAVEN data are publicly available through the Planetary Data System. The source code for the pickup ion model used this study is publicly available at http://goo.gl/Fctdzi.

References

Anderson, D. E. (1974), Mariner 6, 7, and 9 Ultraviolet Spectrometer Experiment: Analysis of hydrogen Lyman alpha data, *J. Geophys. Res., 79*(10), 1513–1518, doi:10.1029/JA079i010p01513.

Barabash, S., E. Dubinin, N. Pissarenko, R. Lundin, and C. T. Russell (1991), Picked-up protons near Mars: Phobos observations, *Geophys. Res. Lett., 18*(10), 1805-1808, doi:10.1029/91GL02082.

Bertucci, C., N. Romanelli, J. Y. Chaufray, D. Gomez, C. Mazelle, M. Delva, R. Modolo, F. González-Galindo, and D. A. Brain (2013), Temporal variability of waves at the proton cyclotron frequency upstream from Mars: Implications for Mars distant hydrogen exosphere, *Geophys. Res. Lett., 40*, 3809–3813, doi:10.1002/grl.50709.

Bhattacharyya, D., J. T. Clarke, J.-L. Bertaux, J.-Y. Chaufray, and M. Mayyasi (2015), A strong seasonal dependence in the Martian hydrogen exosphere, *Geophys. Res. Lett., 42*, 8678–8685, doi:10.1002/2015GL065804.

Bhattacharyya, D., Clarke, J. T., Chaufray, J. Y., Mayyasi, M., Bertaux, J. L., Chaffin, M. S., Villanueva, G. L. (2017), Seasonal changes in hydrogen escape from mars through analysis of HST observations of the Martian exosphere near perihelion. Journal of Geophysical Research: Space Physics, 122., doi:10.1002/2017JA024572.

Bougher, S. W., T. E. Cravens, J. Grebowsky, and J. Luhmann (2014), The aeronomy of Mars: Characterization by MAVEN of the upper atmosphere reservoir that regulates volatile escape, *Space Sci. Rev*., doi:10.1007/s11214-014-0053-7.

Bougher, S. W., et al. (2015), Early MAVEN Deep Dip campaign reveals thermosphere and ionosphere variability, *Science, 350*(6261), doi:10.1126/science.aad0459.

Chaffin, M. S., J.-Y. Chaufray, I. Stewart, F. Montmessin, N. M. Schneider, and J.-L. Bertaux (2014), Unexpected variability of Martian hydrogen escape, *Geophys. Res. Lett., 41*, 314–320, doi:10.1002/2013GL058578.

Chaffin, M. S., et al. (2015), Three-dimensional structure in the Mars H corona revealed by IUVS on MAVEN, *Geophys. Res. Lett., 42*, 9001–9008, doi:10.1002/2015GL065287.

Chaffin, M. S., Deighan, J., Schneider, N. M., & Stewart, A. I. F. (2017), Elevated atmospheric escape of atomic hydrogen from Mars induced by high-altitude water, *Nature Geoscience*, *10*(3), 174-178, doi:10.1038/ngeo2887.

Chamberlain, J. W., and D. M. Hunten (1987), Theory of Planetary Atmospheres: An Introduction to Their Physics and Chemistry, Academic Press, Florida.

Chassefière, E., and F. Leblanc (2004), Mars atmospheric escape and evolution; interaction with the solar wind, *Planet. Space Sci.*, *52*(11), 1039-1058, doi:10.1016/j.pss.2004.07.002.

Chaufray, J. Y., F. Gonzalez-Galindo, F. Forget, M. Lopez-Valverde, F. Leblanc, R. Modolo, and S. Hess (2015), Variability of the hydrogen in the martian upper atmosphere as simulated by a 3D atmosphere–exosphere coupling, *Icarus*, *245*, 282-294, doi:10.1016/j.icarus.2014.08.038.

Clarke, J. T., J.-L. Bertaux, J.-Y. Chaufray, G. R. Gladstone, E. Quemerais, J. K. Wilson, and D. Bhattacharyya (2014), A rapid decrease of the hydrogen corona of Mars, *Geophys. Res. Lett., 41*, 8013–8020, doi:10.1002/2014GL061803.

Clarke, J. T., et al. (2017), Variability of D and H in the Martian Upper Atmosphere Observed with the MAVEN IUVS Echelle Channel, *J. Geophys. Res., 112*, doi:10.1002/2016JA023479.

Connerney, J. E. P., J. Espley, P. Lawton, S. Murphy, J. Odom, R. Oliversen, and D. Sheppard (2015), The MAVEN Magnetic Field Investigation, *Space Sci. Rev.*, doi:10.1007/s11214-015-0169-4.

Cravens, T. E., A. Hoppe, S. A. Ledvina, and S. McKenna-Lawlor (2002), Pickup ions near Mars associated with escaping oxygen atoms, *J. Geophys. Res.*, *107*(A8), doi:10.1029/2001JA000125.

Cravens, T. E., et al. (2016), Hot Oxygen Escape from Mars: Simple Scaling with Solar EUV Irradiance, *J. Geophys. Res., 121*, doi:10.1002/2016JA023461.

Cravens, T. E., O. Hamil, S. Houston, S. Bougher, Y. Ma, D. Brain, and S. Ledvina (2017), Estimates of Ionospheric Transport and Ion Loss at Mars, *Journal of Geophysical Research: Space Physics 122*, 10,626–10,637, doi:10.1002/2017JA024582.

Curry, S. M., M. Liemohn, X. Fang, Y. Ma, and J. Espley (2013), The influence of production mechanisms on pick-up ion loss at Mars, J. Geophys. Res. Space Physics, 118, 554–569, doi:10.1029/2012JA017665.

Deighan, J., et al. (2015), MAVEN IUVS observation of the hot oxygen corona at Mars, *Geophys. Res. Lett., 42*, 9009–9014, doi:10.1002/2015GL065487.

Dong, Y., X. Fang, D. A. Brain, J. P. McFadden, J. S. Halekas, J. E. P. Connerney, F. Eparvier, L. Andersson, D. Mitchell, and B. M. Jakosky (2017), Seasonal variability of Martian ion escape through the plume and tail from MAVEN observations, J. Geophys. Res. Space Physics, 122, 4009–4022, doi:10.1002/2016JA023517.

Dubinin, E., M. Fraenz, J. Woch, S. Barabash, R. Lundin, and M. Yamauchi (2006), Hydrogen exosphere at Mars: Pickup protons and their acceleration at the bow shock, *Geophys. Res. Lett., 33*, L22103, doi:10.1029/2006GL027799.

Dubinin, E., Fraenz, M., Pätzold, M., McFadden, J., Halekas, J. S., DiBraccio, et al. (2017), The effect of solar wind variations on the escape of oxygen ions from Mars through different channels: MAVEN observations, Journal of Geophysical Research: Space Physics, 122, 11,285–11,301, doi:10.1002/2017JA024741.

Eparvier, F. G., P. C. Chamberlin, T. N. Woods, and E. M. B. Thiemann (2015), The solar extreme ultraviolet monitor for MAVEN, *Space Sci. Rev*., doi:10.1007/s11214-015-0195-2

Feldman, P. D., et al. (2011), Rosetta-Alice observations of exospheric hydrogen and oxygen on Mars, *Icarus, 214*, 394-399, doi:10.1016/j.icarus.2011.06.013.

Halekas, J. S., et al. (2015), The solar wind ion analyzer for MAVEN, *Space Sci. Rev*., doi:10.1007/s11214-013-0029-z.

Halekas, J. S., et al. (2017), Structure, dynamics, and seasonal variability of the mars-solar wind interaction: MAVEN solar wind ion analyzer inflight performance and science results, *J. Geophys. Res.*, 121, doi:10.1002/2016JA023167.

Halekas, J. S. (2017), Seasonal variability of the hydrogen exosphere of Mars, *J. Geophys. Res. Planets, 122*, 901–911, doi:10.1002/2017JE005306.

Heavens, N. G., et al. (2018), Hydrogen escape from Mars enhanced by deep convection in dust storms, Nature Astronomy, doi: 10.1038/s41550-017-0353-4.

Hunten, D. M., and M. B. McElroy (1970), Production and escape of hydrogen on Mars, *J. Geophys. Res., 75*(31), 5989–6001, doi:10.1029/JA075i031p05989.

Jakosky, B. M., R. O. Pepin, R. E. Johnson, and J. L. Fox (1994), Mars atmospheric loss and isotopic fractionation by solar-wind-induced sputtering and photochemical escape, *Icarus, 111*(2), 271-288, doi:10.1006/icar.1994.1145.

Jakosky, B. M., et al. (2015a), The Mars Atmosphere and Volatile Evolution (MAVEN) Mission, *Space Sci. Rev*., doi:10.1007/s11214-015-0139-x.

Jakosky, B. M., et al. (2015b), MAVEN observations of the response of Mars to an interplanetary coronal mass ejection, *Science, 350*(6261), doi:10.1126/science.aad0210.

Jakosky, B. M., M. Slipski, M. Benna, P. Mahaffy, M. Elrod, R. Yelle, S. Stone, and N. Alsaeed (2017), Mars' atmospheric history derived from upper-atmosphere measurements of 38Ar/36Ar, *Science* 355, doi:10.1126/science.aai7721.

Johnson, B. C., Liemohn, M. W., Fränz, M., Ramstad, R., Stenberg Wieser, G., & Nilsson, H. (2018), Influence of the interplanetary convective electric field on the distribution of heavy pickup ions around Mars, Journal of Geophysical Research: Space Physics, 123, doi:10.1002/2017JA024463.

Kaneda, K., N. Terada, and S. Machida (2009), Solar-wind control of the hot oxygen corona around Mars, *J. Geophys. Res., 114*, E02007, doi:10.1029/2008JE003234.

Kim, J., A. F. Nagy, J. L. Fox, and T. E. Cravens (1998), Solar cycle variability of hot oxygen atoms at Mars, *J. Geophys. Res., 103*(A12), 29339-29342, doi:10.1029/98JA02727.

Kurokawa, H., K. Kurosawa, and T. Usui (2018), A lower limit of atmospheric pressure on early Mars inferred from nitrogen and argon isotopic compositions, *Icarus* 299, 443-459, doi:10.1016/j.icarus.2017.08.020

Larson, D. E., et al. (2015), The MAVEN solar energetic particle investigation. *Space Sci. Rev*., doi:10.1007/s11214-015-0218-z.

Lee, Y., M. R. Combi, V. Tenishev, S. W. Bougher, J. Deighan, N. M. Schneider, W. E. McClintock, and B. M. Jakosky (2015), A comparison of 3-D model predictions of Mars' oxygen corona with early MAVEN IUVS observations, Geophys. Res. Lett., 42, 9015–9022, doi:10.1002/2015GL065291.

Lillis, R. J., et al. (2015), Characterizing atmospheric escape from Mars today and through time, with MAVEN, *Space Sci. Rev., 195*(1-4), 357-422, doi:10.1007/s11214-015-0165-8

Lillis, R. J., et al. (2016), Photochemical Escape of Oxygen from Mars: first results from MAVEN in situ data, *J. Geophys. Res., 122,* 3815–3836, doi:10.1002/2016JA023525

Luhmann, J. G., R. E. Johnson, and M. H. G. Zhang (1992), Evolutionary impact of sputtering of the Martian atmosphere by O+ pickup ions, Geophysical research letters 19.21, 2151-2154, doi: 10.1029/92GL02485.

Mayyasi, M., Clarke, J., Bhattacharyya, D., Deighan, J., Jain, S., Chaffin, M., … Jakosky, B. (2017), The variability of atmospheric deuterium brightness at Mars: Evidence for seasonal dependence, *Journal of Geophysical Research: Space Physics, 122*, 10,811–10,823, doi:10.1002/2017JA024666.

McFadden, J. P., et al. (2015), MAVEN SupraThermal and Thermal Ion Compostion (STATIC) Instrument, *Space Sci. Rev., 195*, 199-256, doi:10.1007/s11214-015-0175-6.

Mitchell, D. L., et al. (2016), The MAVEN solar wind electron analyzer. *Space Sc. Rev., 200*, 495-528, doi:10.1007/s11214-015-0232-1.

Nagy, A. F., and T. E. Cravens (1988), Hot oxygen atoms in the upper atmospheres of Venus and Mars, *Geophys. Res. Lett., 15*(5), 433-435, doi:10.1029/GL015i005p00433.

Rahmati, A., T. E. Cravens, A. F. Nagy, J. L. Fox, S. W. Bougher, R. J. Lillis, S. A. Ledvina, D. E. Larson, P. Dunn, and J. A. Croxell (2014), Pickup ion measurements by MAVEN: A diagnostic of photochemical oxygen escape from Mars, *Geophys. Res. Lett., 41*, doi:10.1002/2014GL060289.

Rahmati, A., D. E. Larson, T. E. Cravens, R. J. Lillis, P. A. Dunn, J. S. Halekas, J. E. Connerney, F. G. Eparvier, E. M. B. Thiemann, and B. M. Jakosky (2015), MAVEN insights into oxygen pickup ions at Mars, *Geophys. Res. Lett., 42*, doi:10.1002/2015GL065262.

Rahmati, A. (2016), *Oxygen Exosphere of Mars: Evidence from Pickup Ions Measured by MAVEN*, PhD Dissertation, Department of Physics and Astronomy, University of Kansas, ISBN:9781339872629.

Rahmati, A. et al. (2017), MAVEN measured oxygen and hydrogen pickup ions: Probing the Martian exosphere and neutral escape, Journal of Geophysical Research: Space Physics 122, 3689-3706, doi:10.1002/2016JA023371.

Ramstad, R., S. Barabash, Y. Futaana, H. Nilsson, and M. Holmström (2017), Global Mars-solar wind coupling and ion escape, J. Geophys. Res. Space Physics, 122, 8051–8062, doi:10.1002/2017JA024306.

Romanelli, N., et al. (2016), Proton cyclotron waves occurrence rate upstream from Mars observed by MAVEN: Associated variability of the Martian upper atmosphere, *J. Geophys. Res., 121*, doi:10.1002/2016JA023270.

Thiemann, E. M. B., P. C. Chamberlin, F. G. Eparvier, T. N. Woods, S. W. Bougher, and B. M. Jakosky (2017), The MAVEN EUVM model of solar spectral irradiance variability at mars: Algorithms and results, J. Geophys. Res. Space Physics, 122, doi:10.1002/2016JA023512.

Valeille, A., et al. (2009), Three-dimensional study of Mars upper thermosphere/ionosphere and hot oxygen corona: 2. Solar cycle, seasonal variations and evolution over history, J. Geophys. Res., 114, E11006, doi:10.1029/2009JE003389.

Yamauchi M., et al. (2015), Seasonal variation of Martian pick-up ions: Evidence of breathing exosphere, *Planet. Space Sci*., doi:10.1016/j.pss.2015.09.013.

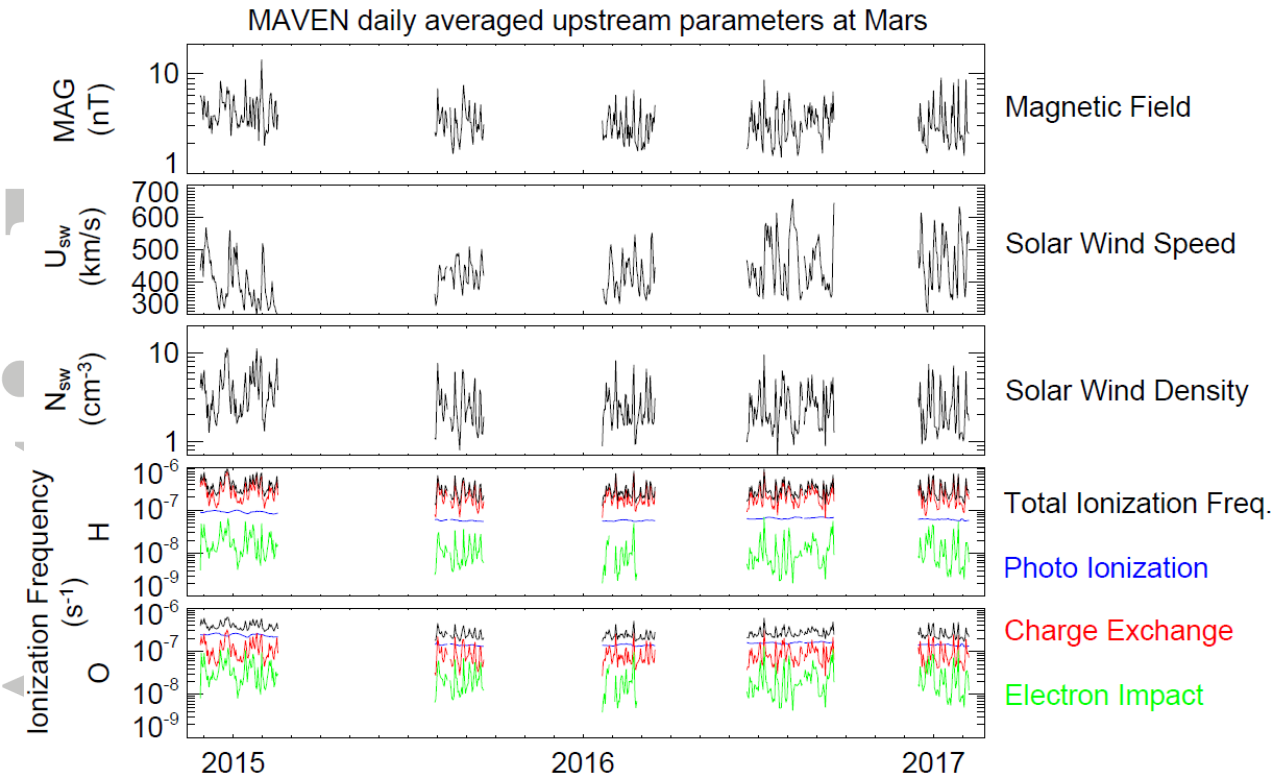

Figure 1. Daily averaged MAVEN measured upstream magnetic field magnitude, solar wind speed, and solar wind density at Mars, along with calculated hydrogen and oxygen ionization frequencies. Charge exchange by solar wind protons and photoionization are the dominant ionization mechanisms for H and O, respectively. Solar wind electron impact is a minor ionization process for both species. The periods with no upstream data are for when no part of MAVEN's orbit was sampling the solar wind.

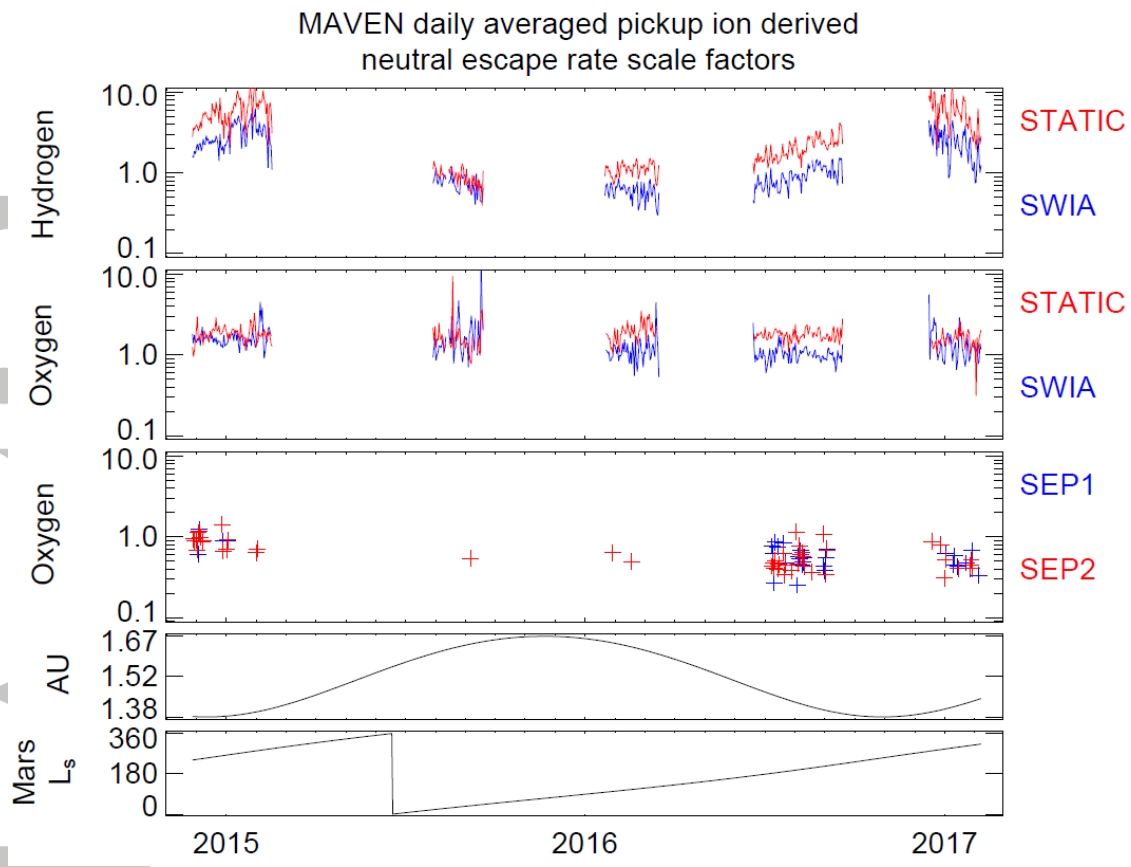

Figure 2. Daily averaged SEP, SWIA, and STATIC derived neutral H and O escape rate scale factors along with Mars heliocentric distance and solar longitude. The scale factors are calculated by taking the ratio between the measured and modeled flux of pickup ions, indicating by how much the assumed input neutral density profiles and therefore the neutral escape rates need to be adjusted to match the data.

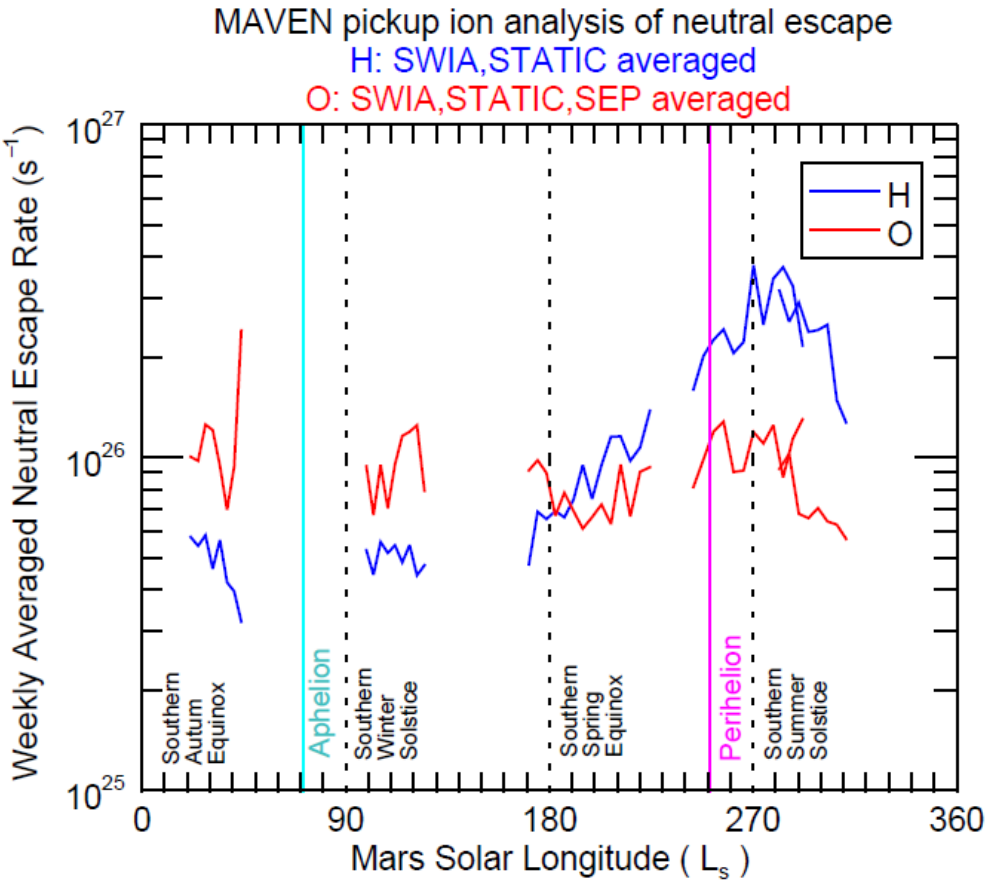

Figure 3. Seasonal variation of neutral H and O escape rates as derived from MAVEN pickup H^+ and O^+ observations. The escape rates are weekly averaged over SWIA and STATIC for H and over SWIA, STATIC, SEP1 and SEP2 for O. The location of aphelion and perihelion along with Mars seasons are also included. A factor of 10 variation in H escape rate is observed, whereas O escape rate remains steadier.

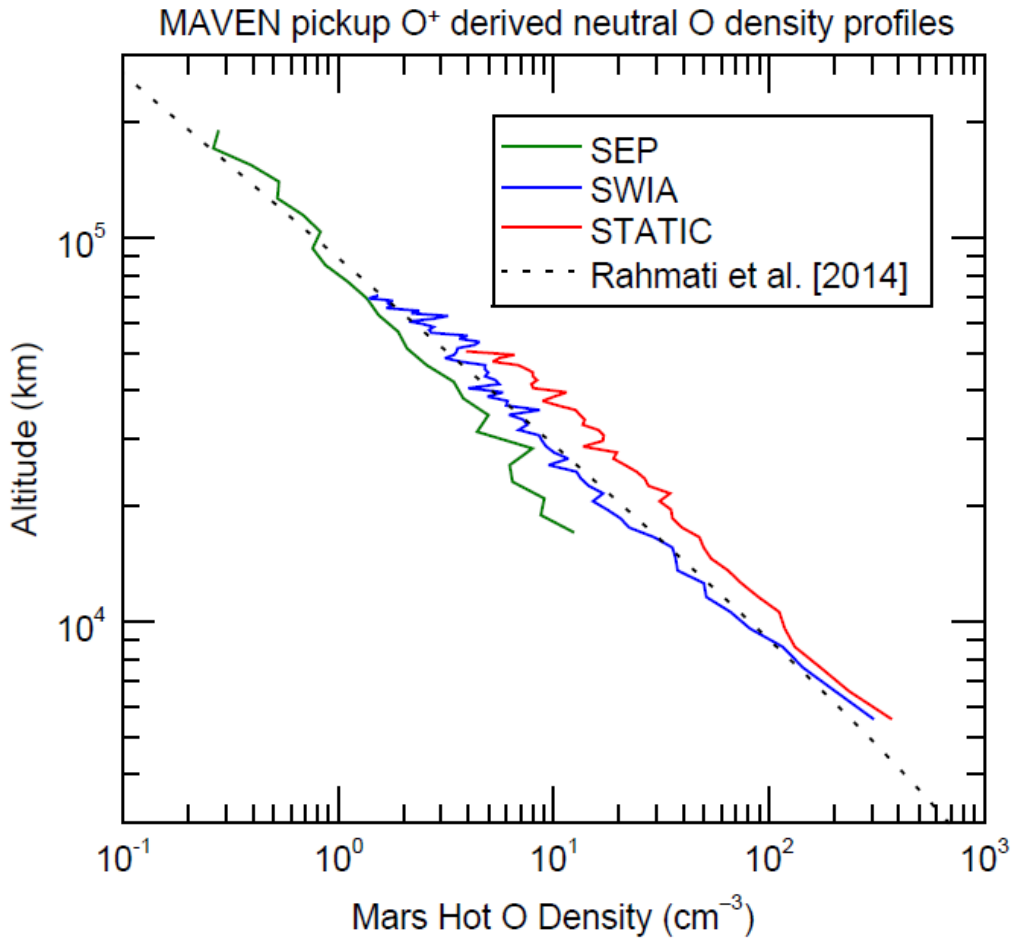

Figure 4. Hot oxygen density profiles derived from SEP, SWIA, and STATIC pickup O^+ measurements by back-tracing the pickup ions to their ionization point in the exosphere. The hot O exospheric density profile of Rahmati et al. [2014] is included for comparison. The factor of 3 disagreement between the densities is most likely due to the lack of reliable calibration between the three instruments at pickup ion energies.